Progress In Electromagnetics Research B, Vol. 81, 81–100, 2018

Solutions of Eddy-Current Problems in a Finite Length Cylinder by Separation of Variables

Yuriy Zhilichev*

Abstract—Magnetic field and eddy currents in a cylinder of finite length are calculated by separation of variables. The magnetic field outside the cylinder or inside the bore of the hollow cylinder and shell is expressed in terms of Bessel functions. Both axial and transverse applied fields are considered for the solid and hollow cylinders. The equations for the vector potential components are transformed in one-dimensional equations along the radial coordinate with the consequent integration by the method of variation of parameters. The equation for the scalar electric potential when required is also integrated analytically. Expressions for the magnetic moment and loss are derived. An alternative analytical solution in terms of scalar magnetic potential is derived for the finite length thin shells. All formulas are validated by the comparison with the solutions by finite-element and finite-difference methods.

1. INTRODUCTION

The paper presents an analytical method of calculation of steady-state magnetic fields and eddy-currents in the cylinder of a finite length placed in the external axial or transverse magnetic field. It is known that for the infinitely long cylinder closed form solutions were known in different forms [1–4]. However as pointed out by many authors [1, 2, 5, 6], for the finite length cylinder the general analytical solution had not been available. For axial symmetry the distribution of eddy currents induced in a conducting rod of finite length by a coaxial coil is given in [7]. In general, the problem of a finite length cylinder earlier was solved by different numerical methods, and the solution was reported by several authors [6, 8–11]. The conductive cylinder in transverse field was also included in so-called FELIX test problems in 80-ties [12, 13] to verify the FEA codes. The analysis of eddy-currents in the cylinder is of interest for many practical applications such as electromagnetic shielding, designs of MRI/NMR components, conductive components of accelerator magnets, fusion reactors, magnetometers, turbogenerators and other electrical machines. The main aim of this paper is to derive a general analytical solution in terms of Bessel functions for eddy currents induced in a conductive cylinder by the quasi-static electromagnetic field. The solution can be used for the fast estimation of magnetic moment, dissipated power, shielding efficiency in structures with conductive circular cylinders. It can also be used as a benchmark when testing codes for calculations of eddy-currents.

2. FORMULATION OF THE PROBLEM

We consider a conductive non-magnetic cylinder with constant electrical conductivity σ and magnetic permeability μ placed in the applied magnetic field oscillating with constant frequency ω. The vector magnetic potential A satisfies Ampere's equation

$$rotrot\vec{A} = \mu_0 \vec{j}, \tag{1}$$

Received 27 April 2018, Accepted 13 June 2018, Scheduled 26 June 2018
* Corresponding author: Yuriy Zhilichev (yzhilichev@netzero.net).
The author is in Durham, NC 27707, USA.

where μ_0 is the magnetic permeability of free space, j the current density for the area $r = [0, r_0]$, $\phi = [0, 2\pi]$, $z = [-z_0, z_0]$ and zero outside this region.

The boundary condition at infinity

$$\vec{A}(\infty) = \vec{A}_0, \tag{2}$$

where A_0 is the vector potential of applied magnetic field.

From Ohm's law, we can express the current density in terms of the vector and scalar V potentials of electromagnetic field as:

$$\vec{j} = -\sigma \frac{\partial \vec{A}}{\partial t} - \sigma \nabla V, \tag{3}$$

where σ is the electrical conductivity of cylinder. The induced currents form the closed loops, and therefore the current density satisfies the condition for the solenoidal field

$$div\vec{j} = 0. \tag{4}$$

The vector potential allows us to apply an additional gauging condition so that the field can be determined uniquely from the Maxwell equations. If we apply Coulomb gauge ($div\vec{A} = 0$) Equations (1) and (4) become

$$\nabla^2 \vec{A} = -\mu_0 \vec{j}, \tag{5}$$

$$\nabla^2 V = 0 \tag{6}$$

with the coupled boundary conditions

$$\frac{\partial V}{\partial n}_{|\Gamma} = -\frac{\partial \vec{A}}{\partial t}\vec{n}. \tag{7}$$

Equation (7) provides a zero component of eddy-currents normal to the surface Γ of the conducive cylinder. The scalar potential is defined to be zero outside the conductor. After substituting Eq. (3) in Eq. (5), we have a system of four differential equations that are coupled. To decouple the equations we can apply Lorentz type of gauge for the vector potential. If we select

$$div\vec{A} = -\mu_0 \sigma V, \tag{8}$$

then Eqs. (1), (4) become

$$\nabla^2 \vec{A} = \mu_0 \sigma \frac{\partial \vec{A}}{\partial t}, \tag{9}$$

$$\nabla^2 V = -div \frac{\partial \vec{A}}{\partial t}. \tag{10}$$

However, outside the cylinder the electrical conductivity σ is zero, and Eq. (8) becomes the Coulomb gauge. Since different gauges are inside and outside the cylinder, we have to satisfy the conditions of continuity for the tangential components of field and normal components of flux density at the cylinder boundaries. Then the components of vector and scalar potentials become coupled again. Therefore, the Lorentz gauge does not help in this case to simplify the problem.

In orthogonal system of coordinates, Equations (9) and (10) can be solved by the method of separation of variables when the boundary Γ coincides with the pieces of coordinates surfaces. A conductive cylinder falls in this category of geometries. However, we have not found in literature the complete analytical solution for the eddy-current problem when the field is applied orthogonal to the cylinder axis. The major obstacle probably is in writing the analytical solution of the field in the whole space outside and inside the cylinder without subdividing the space in sub-regions. However in case of linear conductors, there are no rapid changes of the flux density or field on its boundaries at least for moderate frequencies. Therefore, the vector potential of magnetic field can be sought as a continuous smooth function in the whole space having piecewise conductive properties. The only problem seems to appear for the electric scalar potential that has to be coupled accurately with the vector magnetic potential on the boundaries of the conductor.

3. CYLINDER IN AXIAL FIELD

When cylinder is placed in the axial magnetic field (Fig. 1), the problem can be significantly simplified. Only one component of vector potential is enough to formulate the problem. The scalar electric potential is not needed in this case. The complex azimuthal component of vector potential $A_\phi \exp(i\omega t)$ inside and outside the cylinder satisfies the equation

$$\frac{\partial^2 A_\phi}{\partial r^2} + \frac{1}{r}\frac{\partial A_\phi}{\partial r} - \frac{A_\phi}{r^2} + \frac{\partial^2 A_\phi}{\partial z^2} = -\mu_0 j_\phi, \tag{11}$$

and the far field boundary condition

$$A_\phi(\infty) = B_0 r/2, \tag{12}$$

where B_0 is the amplitude of applied field. The vector potential of uniform field in the form of Eq. (12) can be found by integrating the equation $rot\vec{A} = \vec{B}$ [1, 5].

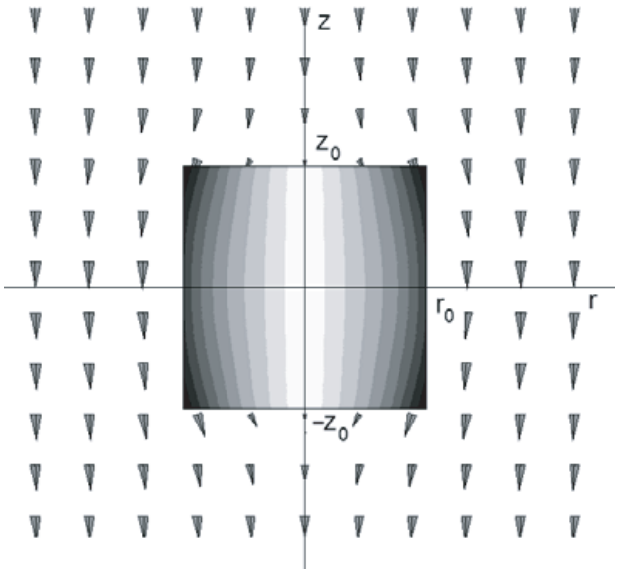

Figure 1. Conductive cylinder of radius r_0 and length $2z_0$ in uniform axial field B_0 directed in z-axis.

The current density in Eq. (11) can be expressed in terms of the time derivative of vector potential

$$j_\phi = -i\omega\sigma A_\phi. \tag{13}$$

Since the magnetic permeability is the same through the whole space, we can express the solution in the form of Fourier series accounting for the field symmetry as

$$A_\phi = \sum_{m=1} A_m(r)\cos\lambda_m z, \tag{14}$$

where $\lambda_m = \pi(2m-1)/(2z_\infty)$; z_∞ is the axial coordinate where the field satisfies the far-field boundary condition in Eq. (12).

In accordance with Grinberg method [14] after substituting Eq. (14) in Eq. (11) and integrating over the interval $[0, z_\infty]$ with the weight $(2/z_\infty)\cos\lambda_m z$, we have

$$\frac{\partial^2 A_m}{\partial r^2} + \frac{1}{r}\frac{\partial A_m}{\partial r} - \frac{A_m}{r^2} - \lambda_m^2 A_m = -\mu_0 j_m, \tag{15}$$

where

$$j_m = -i\sigma\omega \sum_l d_{ml} A_l, \tag{16}$$

$$d_{ml} = \frac{2}{z_\infty}\int_0^{z_0} \cos\lambda_m z \cos\lambda_l z dz = \frac{1}{z_\infty}\left(\frac{\sin(\lambda_m - \lambda_l)z_0}{\lambda_m - \lambda_l} + \frac{\sin(\lambda_m + \lambda_l)z_0}{\lambda_m + \lambda_l}\right). \tag{17}$$

Using a method of variable parameters homogeneous equation and a particular solution of Eq. (15)

$$A_m(r) = \frac{B_0 r d_{m0}}{2} + C_m J_1(i\lambda_m r) + D_m H_1^1(i\lambda_m r) - \frac{\mu_0 \pi}{2i} J_1(i\lambda_m r) \int_r^{r_0} j_m(r') H_1^1(i\lambda_m r') r' dr'$$

$$-\frac{\mu_0 \pi}{2i} H_1^1(i\lambda_m r) \int_0^{r} j_m(r') J_1(i\lambda_m r') r' dr', m \geq 1, \tag{18}$$

where

$$d_{m0} = \frac{2}{z_\infty} \int_0^{z_\infty} \cos \lambda_m z dz = \frac{2}{\lambda_m z_\infty} (-1)^{m+1}, \tag{19}$$

J_1 and H_1^1 are Bessel and Hankel functions, respectively, and C_m and D_m are the constants. To keep the potential finite at $r = 0$, we have to eliminate the functions that have singularities on the cylinder axis. This is achieved by zeroing $D_m = 0$ in Eq. (18). To satisfy the boundary condition in Eq. (12), we have to assume $C_m = 0$ as well. Then, after replacing the functions of complex argument in Eq. (18) by the modified Bessel functions, we rewrite equations for harmonics of vector potential as:

$$A_m(r) = \frac{B_0 r d_{m0}}{2} + \mu_0 I_1(\lambda_m r) \int_r^{r_0} j_m(r') K_1(\lambda_m r') r' dr' + \mu_0 K_1(\lambda_m r) \int_0^{r} j_m(r') I_1(\lambda_m r') r' dr',$$

$$m = 1, \ldots, M. \tag{20}$$

After substituting j_m in Eq. (20) by Eq. (16) and approximating the integrals by the high-accuracy quadrature on the regular grid $r_n = r_{n-1+} h_{rn}$, $n = 1, N$ in the interval $[0, r_0]$, one can derive a system of linear equations for the potential harmonics, $x_k = A_m(r_n)$, $k = n + (m-1)N$:

$$\sum_{k'} c_{kk'} x_{k'} = f_k, \tag{21}$$

where

$$c_{kk'} = \delta_{kk'} + i\mu_0 \sigma \omega h_{rn'} r_{n'} w_n w_{n'} d_{mm'} \left\{ \begin{array}{l} I_1(\lambda_m r_{n'}) K_1(\lambda_m r_n), \ n \geq n' \\ I_1(\lambda_m r_n) K_1(\lambda_m r_{n'}), \ n \leq n' \end{array} \right\}$$
$$f_k = \frac{1}{2} B_0 r_n d_{m0}, \tag{22}$$

w_n are the quadrature weights; h_r is the grid size over the radial coordinate; $\delta_{kk'}$ is the Kronecker delta.

Formulas for harmonics of vector potential in Eq. (20) can be easily modified for the hollow cylinder with the inner radius r_i. The only change required in Eq. (20) (that is now valid for $r \geq r_i$) is the replacement of zero by r_i as a lower limit in all integrals over the radial coordinate. For hollow cylinders, it is of practical interest to calculate the field on the axis. The vector potential inside the bore $0 \leq r \leq r_i$

$$A_m(r) = \frac{B_0 r d_{m0}}{2} + \mu_0 I_1(\lambda_m r) \int_{r_i}^{r_0} j_m(r') K_1(\lambda_m r') r' dr'. \tag{23}$$

The expression for the axial component can be derived as

$$B_z = \sum_{m=1}^{M} B_m(0) \cos \lambda_m z, \tag{24}$$

where coefficients B_m

$$B_m(0) = B_0 d_{m0} - i\mu_0 \sigma \omega \lambda_m \int_{r_i}^{r_0} K_1(\lambda_m r) \sum_{l=1}^{M} d_{ml} A_l(r) r dr, \tag{25}$$

or after approximation the integral by the quadrature

$$B_m(0) = B_0 d_{m0} - i\mu_0\sigma\omega\lambda_m \sum_{n=1}^{N} K_1(\lambda_m r_n) r_n w_n h_{rn} \sum_{l=1}^{M} d_{ml} A_l(r_n), \quad r_1 = r_i,\ r_N = r_0, \tag{26}$$

For the field outside the cylinder, the harmonics of potential are calculated in terms of harmonics on the grid within the cylinder as:

$$A_m(r > r_0) = \frac{B_0 r d_{m0}}{2} - i\mu_0\sigma\omega K_1(\lambda_m r) \sum_{n=1}^{N} I_1(\lambda_m r_n) r_n h_{rn} w_n \sum_{l=1}^{M} d_{ml} A_l(r_n). \tag{27}$$

The radial component of flux density outside the cylinder

$$B_r(r > r_0) = \sum_{m=1}^{M} B_m(r > r_0) \sin \lambda_m z, \tag{28}$$

where

$$B_m(r > r_0) = -i\mu_0\sigma\omega\lambda_m K_1(\lambda_m r) \sum_{n=1}^{N} I_1(\lambda_m r_n) r_n h_{rn} w_n \sum_{l=1}^{M} d_{ml} A_l(r_n). \tag{29}$$

The field inside has a similar structure, but the modified Bessel functions of the first and second kind in Eq. (29) are swapped. The axial component of flux density can be derived as well. In general, it will include $K_1(\lambda_m r)$ and its derivative over the radial coordinate outside the cylinder and $I_1(\lambda_m r)$ and its derivative inside the cylinder if being hollow.

For the thin cylindrical shells, the number of steps over the radial coordinates can be significantly reduced. For just one step the set of Equation (21) degrades to the system of equations for the potential harmonics at the same radial coordinate.

The far-field boundary in Eq. (2) is applied at z_{inf} that is typically selected in the range of $5z_0$ or higher. To reduce the oscillations in the solution, Lanczos smoothing is applied in all series over the axial coordinate.

The total current induced in the cylinder is

$$I_{total} = 2 \int_{r_i}^{r_0} \int_{0}^{z_0} j_\phi dz dr = -2i\sigma\omega \sum_{n=1}^{N} \sum_{m=1}^{M} \frac{w_n d_{rn}}{\lambda_m} A_m(r_n) \sin \lambda_m z_0. \tag{30}$$

The moment of the induced currents is calculated as

$$M_z = 4\pi \int_{r_i}^{r_0} \int_{0}^{z_0} j_\phi r^2 dz dr = -2\pi i\sigma\omega \sum_{n=1}^{N} \sum_{m=1}^{M} \frac{w_n r_n^2}{\lambda_m} h_{rn} A_m(r_n) \sin \lambda_m z_0. \tag{31}$$

The power dissipated in the cylinder is

$$P = \frac{2\pi}{\sigma} \int_{r_i}^{r_0} \int_{0}^{z_0} j_\phi j_\phi^* r dz dr = \frac{\pi z_\infty}{\sigma} \sum_{n=1}^{N} \sum_{m=1}^{M} \sum_{l=1}^{M} d_{ml} j_m j_l^* w_n r_n h_{rn}. \tag{32}$$

Formulas for the field components, moment and power loss have been validated by the comparison with the results from FEA code [15]. The solid and hollow copper cylinders of radius 1 cm and various lengths have been considered. The results of comparison are presented in Fig. 2–Fig. 6. The number of harmonics M in these numerical tests is typically in the range between 20 and 30, and the number of steps in radial grid, N, is between 20 and 30 as well. The step Δ_{rn} depends on the frequency, and it is selected based on the skin depth.

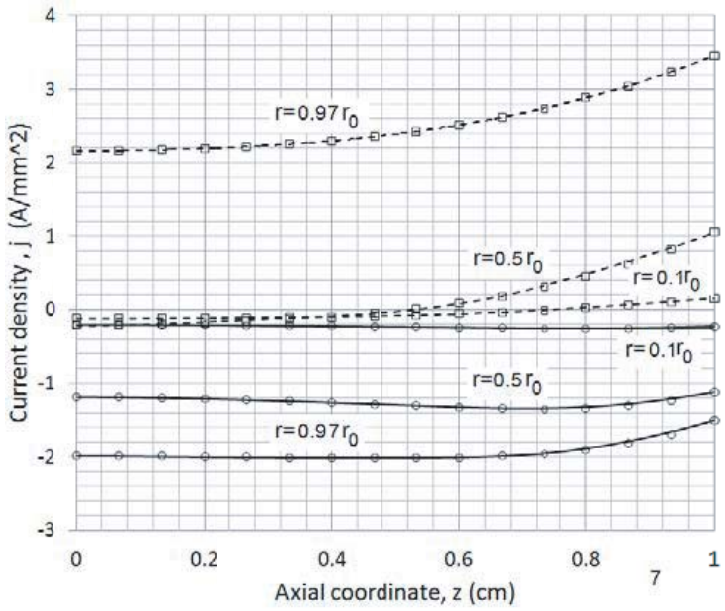

Figure 2. Current density across the cylinder of $r_0 = 1\,\text{cm}$, $z_0 = 1\,\text{cm}$ at $f = 300\,\text{Hz}$, $B_0 = 10\,\text{mT}$: solid line = real$j$, analytical, dash line = imaginary$j$, analytical; $\circ$ = real$j$, FEA, $\square$ = imaginary$j$, FEA.

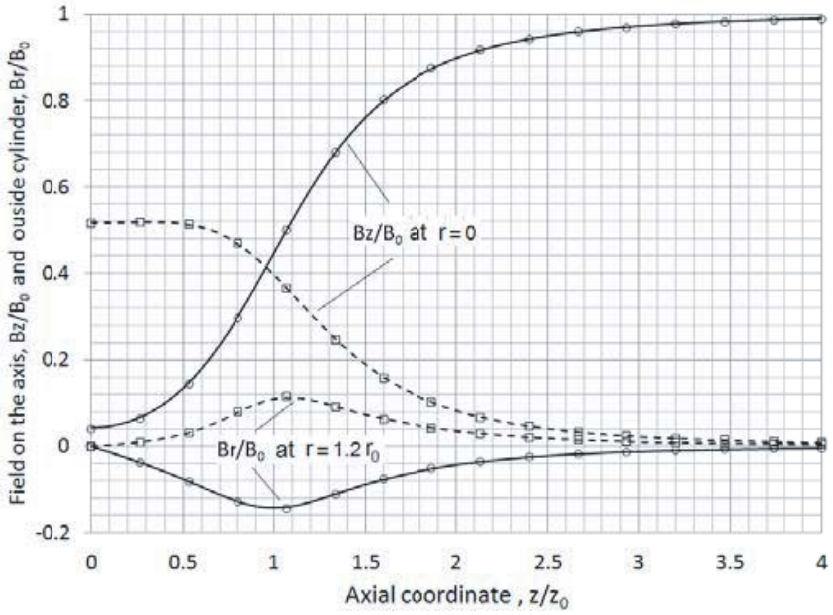

Figure 3. Relative flux density on the axis and outside of the hollow cylinder of $r_i = 0.5\,\text{cm}$, $r_0 = 1\,\text{cm}$, $z_0 = 1\,\text{cm}$ at $f = 300\,\text{Hz}$: solid line = real component, analytics, dash line = imaginary component, analytics; $\circ$ = real component, FEA, $\square$ = imaginary component, FEA.

4. CYLINDER IN TRANSVERSE FIELD

4.1. Solid Cylinder

Let's assume that the external field is applied in x-direction (Fig. 7). The vector magnetic potential has all three components A_r, A_ϕ, A_z. The potential satisfies Eq. (5) in the whole space when Coulomb gauge is selected. The current density is non-zero for the area $r = [0, r_0]$, $\phi = [0, 2\pi]$, $z = [-z_0, z_0]$, and

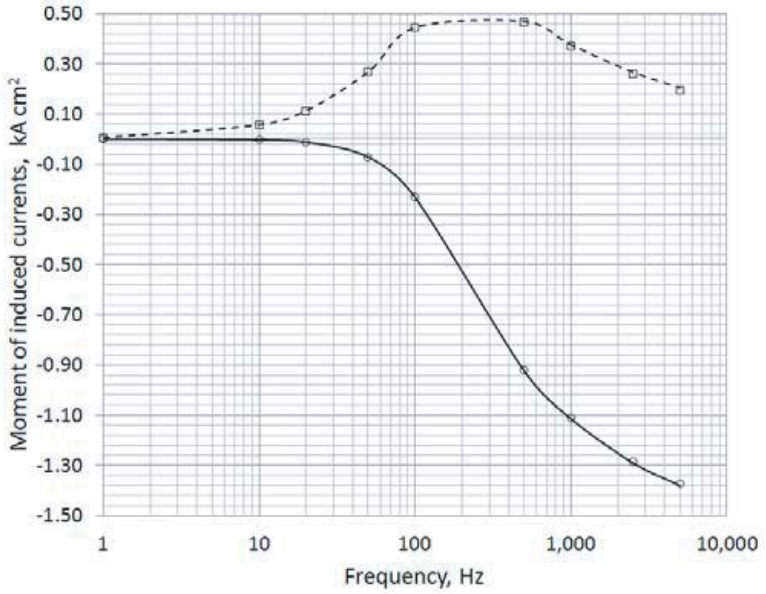

Figure 4. Moment of currents induced in the solid cylinder of $r_0 = 1\,\text{cm}$, $z_0 = 1\,\text{cm}$ at $B_0 = 10\,\text{mT}$ of axial field: solid line = real component, analytics, dash line =imaginary component, analytical; $\circ$ = real component, FEA, $\square$ = imaginary component, FEA.

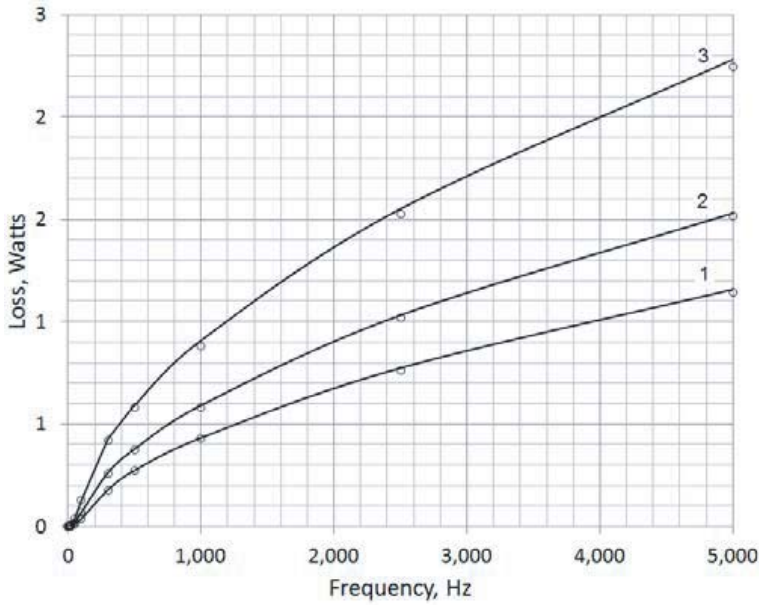

Figure 5. Power loss in the hollow cylinder of $r_i = 0.5\,\text{cm}$, $r_0 = 1\,\text{cm}$ in the applied field of $B_0 = 10\,\text{mT}$ at different lengths, $2z_0 = 1\,\text{cm}$ (1); $= 2\,\text{cm}$ (2); $= 4\,\text{cm}$ (3): solid line = analytical solution (21), $\circ$ = FEA.

is zero outside this region. The boundary condition at infinity

$$A_z(\infty) = B_0 r \sin\phi. \tag{33}$$

Equation (5) in the component notation can be written as

$$\nabla^2 A_r - \frac{A_r}{r^2} - \frac{2}{r^2}\frac{\partial A_\phi}{\partial \phi} = -\mu j_r, \tag{34}$$

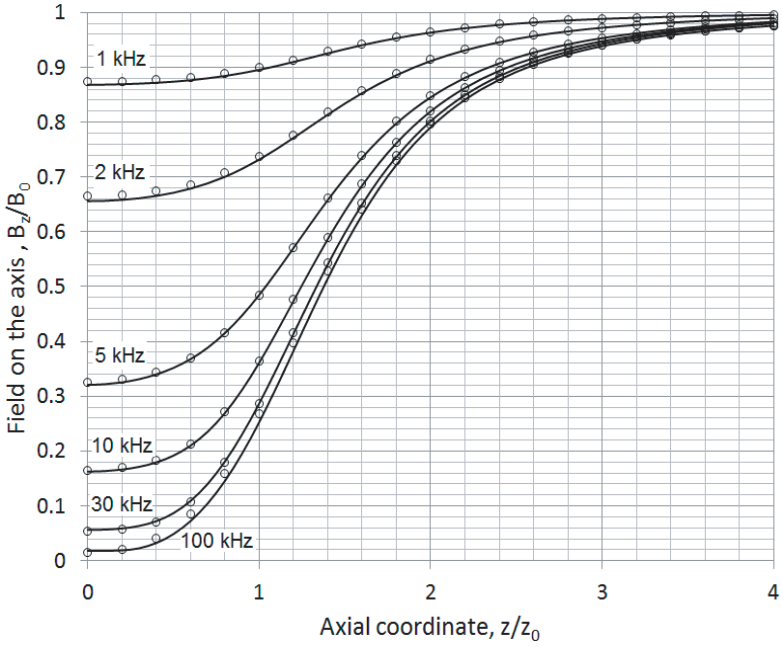

Figure 6. Relative amplitude of flux density on the axis of the thin cylindrical shell of $r_0 = 1\,\text{cm}$, $z_0 = 1\,\text{cm}$, thickness $h_r = 0.35\,\text{mm}$ at different frequencies: solid line = analytics, ∘ = FEA.

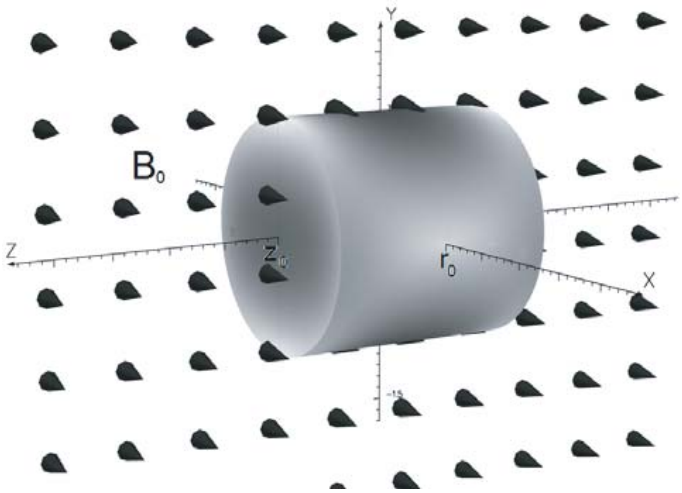

Figure 7. Conductive cylinder of radius r_0 and axial length $2z_0$ in uniform transverse field directed in x-axis.

$$\nabla^2 A_\phi - \frac{A_\phi}{r^2} + \frac{2}{r^2}\frac{\partial A_r}{\partial \phi} = -\mu j_\phi, \tag{35}$$

$$\nabla^2 A_z = -\mu j_z, \tag{36}$$

where $\nabla^2 = \frac{\partial^2}{\partial r^2} + \frac{1}{r}\frac{\partial}{\partial r} + \frac{1}{r^2}\frac{\partial^2}{\partial \phi^2} + \frac{\partial^2}{\partial z^2}$.

The scalar electric potential is also required to satisfy Eq. (6).

Because the magnetic field has a tangential symmetry over xz- and xy-planes and normal symmetry over zy-plane, the potential components can be presented as

$$A_r = \mathrm{A}_r(r,z)\sin\phi, \quad \mathrm{A}_r(r,z) = \sum_{m=1} A_{rm}(r)\sin\lambda_m z, \tag{37}$$

$$A_\phi = \mathrm{A}_\phi(r,z)\cos\phi, \quad \mathrm{A}_\phi(r,z) = \sum_{m=1} A_{\phi m}(r)\sin\lambda_m z, \tag{38}$$

$$A_z = \mathrm{A}_z(r,z)\sin\phi, \quad \mathrm{A}_z(r,z) = \sum_{m=1} A_{zm}(r)\cos\lambda_m z, \tag{39}$$

where $\lambda_m = \pi(2m-1)/(2z_\infty)$.

Since the cylinder has a finite length of $L = 2z_0$, the current density and electric scalar potential are zero beyond its volume while the magnetic field should be extended in z-direction far enough from the cylinder top and base faces. We assume that the magnetic field is equal to the applied field at $z_\infty \le z \ge z_\infty$. Thus the current density and electric potential are expanded in the Fourier series over the interval $z = [-z_0, z_0]$ while the vector potential is fit in the interval $z = [-z_\infty, z_\infty]$. For the current density and electric scalar potential of the cylinder, we also account for the model symmetry

$$j_r = \Im_r \sin\phi, \quad \Im_r = \sum_{l=1} j_{rl}(r)\sin\eta_l z, \tag{40}$$

$$j_\phi = \Im_\phi \cos\phi, \quad \Im_\phi = \sum_{l=1} j_{\phi l}(r)\sin\eta_l z, \tag{41}$$

$$j_z = \Im_z \sin\phi, \quad \Im_z = \sum_{l=1} j_{zl}(r)\cos\eta_l z, \tag{42}$$

$$V = \upsilon \sin\phi, \quad \upsilon = \sum_{k=1} V_k(r)\sin\eta_k z, \tag{43}$$

where $\eta_k = \pi(2k-1)/(2z_0)$.

Equation (36) contains only one component of vector potential and can be solved similar to Eq. (11). After substituting series (39) in (36) and integrating over $[-z_\infty, z_\infty]$, the equation for the potential harmonics is

$$\frac{\partial^2 A_{zm}}{\partial r^2} + \frac{1}{r}\frac{\partial A_{zm}}{\partial r} - \frac{A_{zm}}{r^2} - \lambda_m^2 A_{zm} = -\mu_0 \tilde{j}_{zm}, \tag{44}$$

where

$$\tilde{j}_{zm} = \sum_l a_{ml} j_{zl}, \tag{45}$$

$$a_{ml} = \frac{1}{z_\infty}\int_{-z_0}^{z_0} \cos\lambda_m z \cos\eta_l z dz = \frac{(-1)^l}{z_\infty}\frac{2\eta_l}{\lambda_m^2 - \eta_l^2}\cos\frac{\pi(2m-1)z_0}{2z_\infty}, \quad m,l \ge 1. \tag{46}$$

Similarly to the solution of Eq. (15), we can resolve Eq. (44) in the sum of a general solution of the homogeneous equation and a particular solution. Because the current density harmonics in Eq. (30) are dependent on the radial coordinate, we use the method of variable parameters to express the harmonics A_{zm} in the form of integrals

$$A_{zm} = -B_0 r d_{m0} + \mu_0 I_1(\lambda_m r)\int_r^{r_0} \tilde{j}_{zm}(r')K_1(\lambda_m r')r'dr' + \mu_0 K_1(\lambda_m r)\int_0^r \tilde{j}_{zm}(r')I_1(\lambda_m r')r'dr', \quad m \ge 1. \tag{47}$$

Equations (34) and (35) for the radial and angular components of vector potential contain crossing terms. To avoid coupling between the equations, a few manipulations on Eqs. (34) and (35) should be performed. First, let's exclude the polar angle from the consideration by substituting A_r, A_ϕ into Eqs. (34) and (35) in accordance with Eqs. (38)–(39), respectively

$$\Delta \mathrm{A}_r - \frac{2\mathrm{A}_r}{r^2} + \frac{2\mathrm{A}_\phi}{r^2} = -\mu_0 \Im_r, \tag{48}$$

$$\Delta \mathrm{A}_\phi - \frac{2\mathrm{A}_\phi}{r^2} + \frac{2\mathrm{A}_r}{r^2} = -\mu_0 \Im_\phi, \tag{49}$$

where $\Delta = \frac{\partial^2}{\partial r^2} + \frac{1}{r}\frac{\partial}{\partial r} + \frac{\partial^2}{\partial z^2}$.

Next, we combine Eqs. (48) and (49), namely we add and subtract them from each other to obtain the equations for the new variables $\mathrm{A}_{\phi+r} = \mathrm{A}_\phi + \mathrm{A}_r$ and $\mathrm{A}_{\phi-r} = \mathrm{A}_\phi - \mathrm{A}_r$

$$\Delta \mathrm{A}_{\phi+r} = -\mu_0(\Im_\phi + \Im_r), \tag{50}$$

$$\Delta \mathrm{A}_{\phi-r} - \frac{4\mathrm{A}_{\phi-r}}{r^2} = -\mu_0(\Im_\phi - \Im_r). \tag{51}$$

Note that the variables $\mathrm{A}_{\phi+r}$ and $\mathrm{A}_{\phi-r}$ in Eqs. (50) and (51) are decoupled now, and the solutions can be expressed in terms of Bessel functions of integer index. After multiplying Eqs. (50) and (51) by $1/z_\infty \sin\lambda_m z$ and integrating over $[-z_\infty, z_\infty]$ the equations for the harmonics are

$$\frac{\partial^2 A_{\phi+r,m}}{\partial r^2} + \frac{1}{r}\frac{\partial A_{\phi+r,m}}{\partial r} - \lambda_m^2 A_{\phi+r,m} = -\mu_0\left(\tilde{j}_{rm} + \tilde{j}_{\phi m}\right), \tag{52}$$

$$\frac{\partial^2 A_{\phi-r,m}}{\partial r^2} + \frac{1}{r}\frac{\partial A_{\phi-r,m}}{\partial r} - \frac{4A_{\phi-r,m}}{r^2} - \lambda_m^2 A_{\phi-r,m} = -\mu_0\left(\tilde{j}_{\phi m} - \tilde{j}_{rm}\right), \tag{53}$$

where

$$A_{\phi\pm r,m} = A_{\phi,m} \pm A_{\phi-r,m}, \tag{54}$$

$$\tilde{j}_{\phi m} = \sum_l b_{ml} j_{\phi l}, \tag{55}$$

$$\tilde{j}_{rm} = \sum_l b_{ml} j_{rl}, \tag{56}$$

$$b_{ml} = \frac{1}{z_\infty}\int_{-z_0}^{z_0} \sin\lambda_m z \sin\eta_l z dz = \frac{(-1)^l}{z_\infty}\frac{2\lambda_m}{\lambda_m^2 - \eta_l^2}\cos\frac{\pi(2m-1)z_0}{2z_\infty}, \quad m,l \geq 1. \tag{57}$$

The solution of one-dimensional Equations (52) and (53) can be written in terms of Bessel functions similar to solution of Eq. (47)

$$\begin{aligned} A_{\phi+r,m} = {} & \mu_0 I_0(\lambda_m r)\int_r^{r_0}\left(\tilde{j}_{\phi m}(r') + (\tilde{j}_{rm}(r'))\right) K_0\left(\lambda_m r'\right) r' dr' \\ & + \mu_0 K_0(\lambda_m r)\int_0^{r}\left(\tilde{j}_{\phi m}\left(r'\right) + (\tilde{j}_{rm}\left(r'\right)\right) I_0(\lambda_m r') r' dr' \quad m \geq 1, \end{aligned} \tag{58}$$

$$\begin{aligned} A_{\phi-r,m} = {} & \mu_0 I_2(\lambda_m r)\int_r^{r_0}\left(\tilde{j}_{\phi m}\left(r'\right) - (\tilde{j}_{rm}\left(r'\right)\right) K_2(\lambda_m r') r' dr' \\ & + \mu_0 K_2(\lambda_m r)\int_0^{r}(\tilde{j}_{\phi m}(r') - (\tilde{j}_{rm}(r')) I_2(\lambda_m r') r' dr' \quad m \geq 1. \end{aligned} \tag{59}$$

The current density harmonics $j_{rm}, j_{\phi m}, j_{zm}$ in Eqs. (47), (58), and (59) can be determined from the condition for the divergence-free current density in Eq. (4). Let's impose the Coulomb gauge for the vector potential. Then the scalar electric potential satisfies the Laplace Equation (6). After substituting Eq. (43) in Eq. (6), multiplying it by $1/z_0 \sin\eta_k z$ and integrating over $[-z_0, z_0]$, the equations for the harmonics of scalar potential are

$$\frac{\partial^2 V_k}{\partial r^2} + \frac{1}{r}\frac{\partial V_k}{\partial r} - \frac{V_k}{r^2} - \eta_k^2 V_k = q_k, \tag{60}$$

where the right part of Eq. (60) appears because the normal derivative of scalar potential on the cylinder surface at $z = \pm z_0$ is different from zero. It can be further expressed through the time derivative of

vector potential in accordance with Eq. (7)

$$q_k = -\frac{2(-1)^{k+1}}{z_0}\frac{\partial v}{\partial z}\,|_{z=z_0} = (-1)^k\frac{2i\omega}{z_0}\mathrm{A}_z(z_0). \tag{61}$$

The boundary conditions for the harmonics of scalar potential are

$$V_k(0) = 0, \tag{62}$$

$$\frac{\partial V_k}{\partial r}_{|r=r_0} = -i\omega\tilde{A}_{rk}(r_0), \tag{63}$$

where

$$\tilde{A}_{rk}(r_0) = \frac{z_\infty}{z_0}\sum_m b_{km}A_{rm}(r_0). \tag{64}$$

Note that the boundary condition for the derivative of scalar potential in Eq. (63) is a result of zero radial component of current density at $r = r_0$. In general, Eq. (60) can be resolved through the integrals similar to Eq. (20)

$$V_k = G_kI_1(\eta_k r) + i\omega I_1(\eta_k r)\int_r^{r_0} q_k(r')K_1(\eta_k r')r'dr' + i\omega K_1(\eta_k r)\int_0^{r} q_k(r')I_1(\eta_k r')r'dr', \tag{65}$$

where coefficients G_k are determined from the boundary condition in Eq. (62) as:

$$G_k = -\frac{i\omega}{\eta_k I_1'(\eta_k r_0)}(\tilde{A}_{rm}(r_0) + K_1'(\eta_k r_0)\int_0^{r_0} q_k I_1(\eta_k r')r'dr'), \tag{66}$$

where I_1', K_1' are the first derivatives of Bessel functions.

The scalar potential derivative at $z = \pm z_0$ can be expressed through $\sigma^{-1}div\sigma\vec{A}$. Indeed Eq. (4) can be rewritten as:

$$\nabla^2 V = -\frac{i\omega}{\sigma}div\sigma\vec{A}. \tag{67}$$

The divergence in the right part of Eq. (67) is not zero anymore if we take the ends of cylinder into consideration. For the Coulomb gauge $div\sigma\vec{A}$ is zero everywhere inside the cylinder but the surface where it has a jump of $\sigma(\vec{A}\vec{n})$ that is called as a surface divergence [16]. Because the conductivity is discontinuous at $z = \pm z_0$ and the integration totally includes the jump of σ we have

$$\frac{1}{z_0}\int_{-z_0}^{z_0} div\left(\sigma\vec{A}\right)\sin\eta_k z dz = \frac{1}{z_0}\int_{-z_0}^{z_0} A_z\frac{\partial\sigma}{\partial z}\sin\eta_k z dz = \frac{2(1)^{k+1}}{z_0}\sigma A_z(z_0). \tag{68}$$

Thus the right part in Eq. (60) can be replaced by the integral of $div\sigma\vec{A}$ after accounting for the angular dependence of vector potential components in Eqs. (37)–(39)

$$q_k = \frac{-i\omega}{z_0\sigma}\int_{-z_0}^{z_0}\left[\frac{\partial(\sigma\mathrm{A}_r)}{\partial r} + \frac{\partial(\sigma\mathrm{A}_z)}{\partial z} + \frac{\sigma(\mathrm{A}_r - \mathrm{A}_\phi)}{r}\right]\sin\eta_k z dz. \tag{69}$$

After replacing the vector potential components by harmonics over the axial coordinate and subsequent integration, we obtain

$$q_k = -i\omega\left(\frac{\partial\tilde{A}_{rk}}{\partial r} - \frac{\tilde{A}_{\phi-r,k}}{r} - \eta_k\tilde{A}_{zk}\right), \tag{70}$$

where

$$\tilde{A}_{\phi-r,k} = \frac{z_\infty}{z_0}\sum_m b_{mk}A_{\phi-r,m}, \quad \tilde{A}_{zk} = \frac{z_\infty}{z_0}\sum_m a_{mk}A_{zm}. \tag{71}$$

The coefficients $\tilde{A}_{zk}$ are the result of fitting the axial component A_z to the cosine harmonics along the cylinder length. We use values of potential up to the ends of the interval $[-z_0, z_0]$ where $-i\sigma\omega\mathrm{A}_z$ is zeroed because of the jump in the conductivity. This allows us to account for the surface divergence at $z = \pm z_0$. The computation of q_k using Eq. (70) is more complex than using a straight expression (61). However, including $div\sigma\vec{A}$ in the equation for the scalar potential enforces the divergence-free condition in Eq. (4). To combine the advantages of two methods for computation of q_k, one can add $div\vec{A}$ $(= 0)$ to the jump of potential in expression (61)

$$q_k = (-1)^k \frac{2i\omega}{z_0}\mathrm{A}_z(z_0) + i\omega\frac{z_\infty}{z_0}\sum_l \left(\frac{\partial A_{rl}}{\partial r} - \frac{A_{\phi-r,l}}{r} - \lambda_l A_{zl}\right) b_{kl}. \tag{72}$$

The latter expression for q_k accurately includes the surface divergence and enforces (4) at the same time.

The harmonics of current density can be expressed through the harmonics of potentials as follows:

$$\begin{aligned} j_{rk} &= -\sigma\left(i\omega\tilde{A}_{rk} + \frac{\partial V_k}{\partial r}\right), \\ j_{\phi k} &= -\sigma\left(i\omega\tilde{A}_{\phi k} + \frac{V_k}{r}\right), \\ j_{zk} &= -\sigma\left(i\omega\tilde{A}_{zk} + \eta_k V_k\right). \end{aligned} \tag{73}$$

The solutions in Eqs. (47), (58), (59) and (65) contain the unknown coefficients of harmonics $A_{r+\phi,m}\, A_{\phi-r,m}$, A_{zm}, V_k. After approximation of the integrals by a high accuracy quadratures on the grid $r_n = r_{n-1+}h_{rn}$, $n = 1, N$ built for the interval $[0, r_0]$, these expressions form a system of linear equations of order of $4NM$ where M is the number of harmonics in series (37)–(39), (43). The structure of the system is similar to Eq. (21), but it is more complex since the current density components in Eqs. (47), (58), (59) should be expressed through the vector and scalar potential harmonics using Eq. (73). To simplify the solution, the system of equations can be solved also using the iterative approach. In this case, the current density in Eq. (73) is split so that the parts associated with the time derivatives of vector potential are included into the matrix coefficients while the terms associated with the electric potential are kept in the right part of system.

The analytical method has been applied to the copper cylinder of radius, r_0 of 1 cm, and half length, z_0 of 1 cm. The number of harmonics M has been selected in the range ≥ 30, and the far-field boundary conditions have been applied at $z \geq 3z_0$. The distribution of current density is presented in Fig. 8 in comparison with the results from FEA [15] and FDM [17]. A pure hexahedral mesh in all directions has been used in both numerical methods. The mesh has been refined in both methods until they provide the close solutions in terms of local fields, energy and moment of induced currents. For FDM, the symmetry over the polar angle in Eqs. (37)–(39) has been used first, and then four coupled 2-D equations have been solved. 2-D equations have been approximated using the integral-interpolation method [17]. The finite-differential schemes for the equations are similar to those reported in [18].

4.2. Hollow Cylinder

Similar to the cylinder in the axial field, the calculation formulas for the transverse field can be applied in the case of the hollow cylinder with inner radius r_i, outer radius r_0 and axial length $2z_0$. The equations for the components of vector potential in Eqs. (47), (58)–(59) differ only by the integration range. The lower zero limits in integrals of Eqs. (47), (58)–(59) should be replaced by r_i. Thus the grid along the radial coordinate is built in the interval $[r_i, r_0]$. The expression for the scalar electric potential contains an additional Bessel function of second kind $K_1(\eta_k r)$ with the constant coefficients

$$V_k = G_k I_1(\eta_k r) + F_k K_1(\eta_k r) + I_1(\eta_k r)\int_r^{r_0} q_k\left(r'\right) K_1\left(\eta_k r'\right) r' dr' + K_1(\eta_k r)\int_{r_i}^{r} q_k\left(r'\right) I_1\left(\eta_k r'\right) r' dr'. \tag{74}$$

This is because the scalar potential is considered for $r > 0$. Thus the solution in Eq. (74) that includes infinite functions $K_1(\eta_k r)$ at $r = 0$ is finite everywhere in the hollow cylinder. The boundary condition

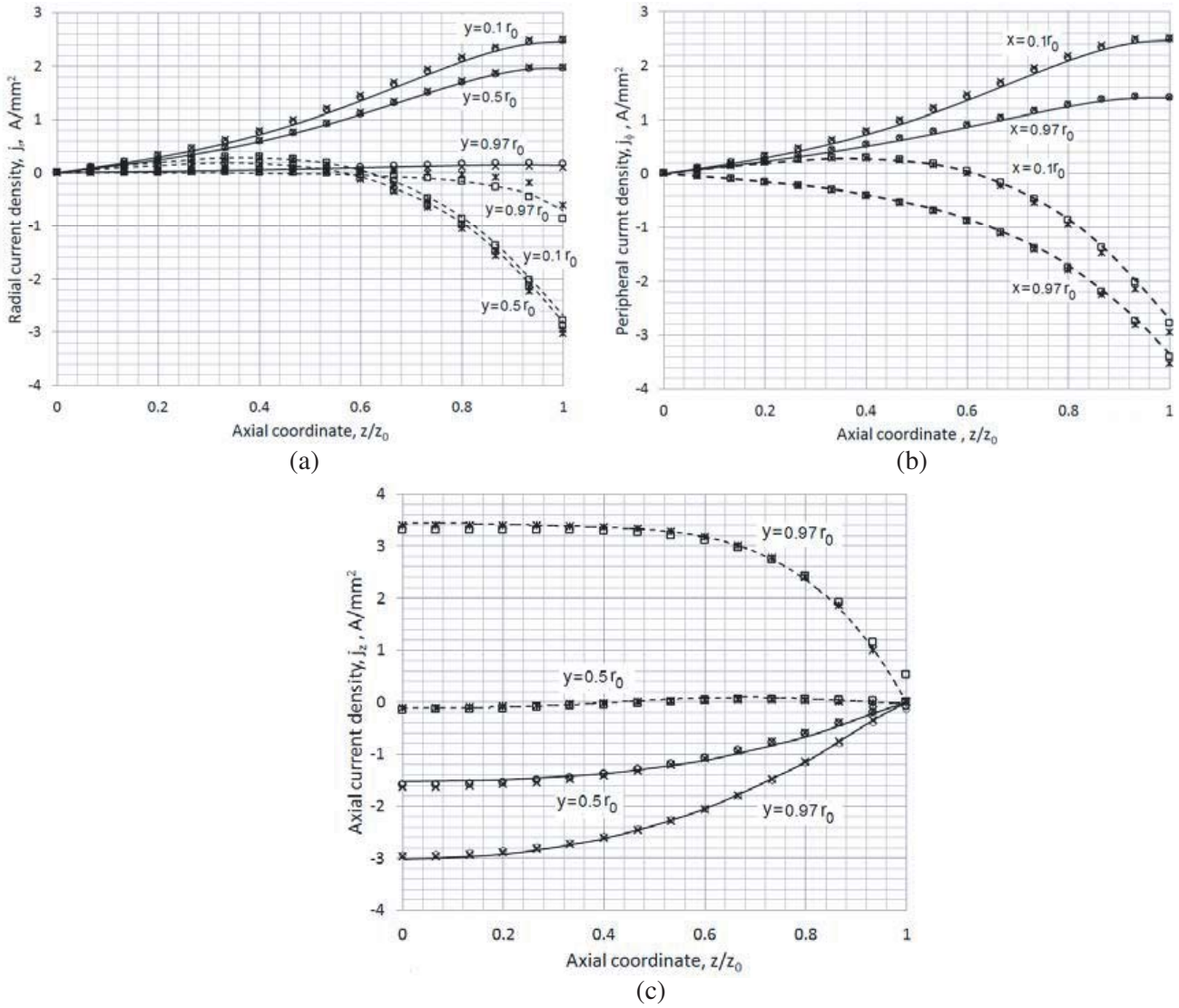

Figure 8. (a) Radial component of current density in YZ-plane, (b) peripheral component of current density in XZ-plane and (c) axial component of current density in YZ-plane across the cylinder of $r_0 = 1\,\text{cm}$, $z_0 = 1\,\text{cm}$ at $f = 300\,\text{Hz}$, $B_0 = 10\,\text{mT}$: solid line = realj_r, analytics, dash line = imaginaryj_r, analytics; $\circ$ = realj_r, FEA, $\square$ = imaginaryj_r, FEA; $\times$ = realj_r, FDM, $*$ = imaginaryj_r, FDM.

on the outer surface of the hollow cylinder is the same as Eq. (63). Similarly, on the inner surface we have

$$\frac{\partial V_k}{\partial r}_{|r=r_i} = -i\omega\tilde{A}_{kr}(r_i). \tag{75}$$

Coefficients G_k and F_k are determined from the boundary condition system in Eqs. (63) and (75) as

$$G_k = \left(K_k'(\eta_k r_0)g_k - K_k'(\eta_k r_i)f_k\right)/D_k, \tag{76}$$

$$F_k = \left(I_k'(\eta_k r_0)f_k - I_k'(\eta_k r_i)g_k\right)/D_k, \tag{77}$$

where

$$g_k = -i\omega\tilde{A}_{rk}(r_0)/\eta_k - K_1'(\eta_k r_0)\int_{r_i}^{r_0} q_k I_1\left(\eta_k r'\right) r' dr', \tag{78}$$

$$f_k = -i\omega\tilde{A}_{rk}(r_i)/\eta_k - I_1'(\eta_k r_i)\int_{r_i}^{r_0} q_k K_1\left(\eta_k r'\right) r' dr', \tag{79}$$

$$D_k = I_k'(\eta_k r_0)K_k'(\eta_k r_i) - I_k'(\eta_k r_i)K_k'(\eta_k r_0). \tag{80}$$

The harmonics of A_z in the bore of the cylinder

$$A_{zm}\,|_{r\le r_i} = -B_0 r d_{m0} + \mu_0 I_1(\lambda_m r)\int_{r_i}^{r_0} \tilde{j}_{zm}\left(r'\right) K_1\left(\lambda_m r'\right) r' dr'. \tag{81}$$

For A_ϕ one can derive

$$\begin{aligned} A_{\phi m}\,|_{r\le r_i} &= \frac{\mu_0}{2} I_0(\lambda_m r)\int_{r_i}^{r_0} \left[\tilde{j}_{\phi m}\left(r'\right) + \tilde{j}_{rm}\left(r'\right)\right] K_0\left(\lambda_m r'\right) r' dr' \\ &+ \frac{\mu_0}{2} I_2(\lambda_m r)\int_{r_i}^{r_0} \left[\tilde{j}_{\phi m}\left(r'\right) - \tilde{j}_{rm}\left(r'\right)\right] K_2\left(\lambda_m r'\right) r' dr'. \end{aligned} \tag{82}$$

The component B_x on z-axis is

$$B_x = \frac{1}{r}\frac{\partial A_z}{\partial \phi} - \frac{\partial A_\phi}{\partial z}, \tag{83}$$

Combining Eqs. (81)–(83) we obtain the flux density on the axis of the cylinder

$$\begin{aligned} B_x\,|_{x;y=0} &= -B_0 + \frac{\mu_0}{2}\sum_m \lambda_m \cos(\lambda_m z)\left[\int_{r_i}^{r_0} \tilde{j}_{zm}(r') K_1(\lambda_m r') r' dr'\right. \\ &\left. - \int_{r_i}^{r_0} (\tilde{j}_{rm}(r') + \tilde{j}_{\phi m}(r')) K_0(\lambda_m r') r' dr'\right]. \end{aligned} \tag{84}$$

Other components are zero on the axis of the cylinder, thus B_x gives us the magnitude of the field on z-axis.

Similar to the solid cylinder, the formulas for the hollow cylinder have been verified by the comparison with the induced currents computed by numerical methods (Fig. 9–Fig. 10) in the range of frequencies. The steps in the radial grid have been selected based on the frequency of the applied field. For example, at least 30 steps ($N = 31$) over the radial coordinate are used for the frequency of 2 kHz in the case study with the results presented in Fig. 10.

4.3. Cylindrical Shell

A cylindrical shell is a special case of the hollow cylinder when we can neglect a radial dependence of current density [2]. First, consider how the thin shell approximation can simplify the solution in the case of hollow cylinder. Since the thickness of the shell typically is significantly less than its radius, it is practical to consider a one-layer ($N = 1$) approximation for the derived solution. Indeed if we neglect the dependence of electric scalar on the radial coordinate, from Eq. (41) we can derive

$$V_k(r_0) = -\frac{q_k}{1/r_0^2 + \eta_k^2}. \tag{85}$$

This simple approach has a few limits. A one-layer approximation totally ignores the difference in the current density across the shell thickness although it accounts for the radial component of vector potential, and hence for the radial current density associated with its time derivative. Also the one-layer model may lead to the ill-defined matrix for the harmonics of vector potential starting at high frequencies. It is illustrated in Fig. 11 for a 0.35 mm thick copper shell of 1 cm radius. When the

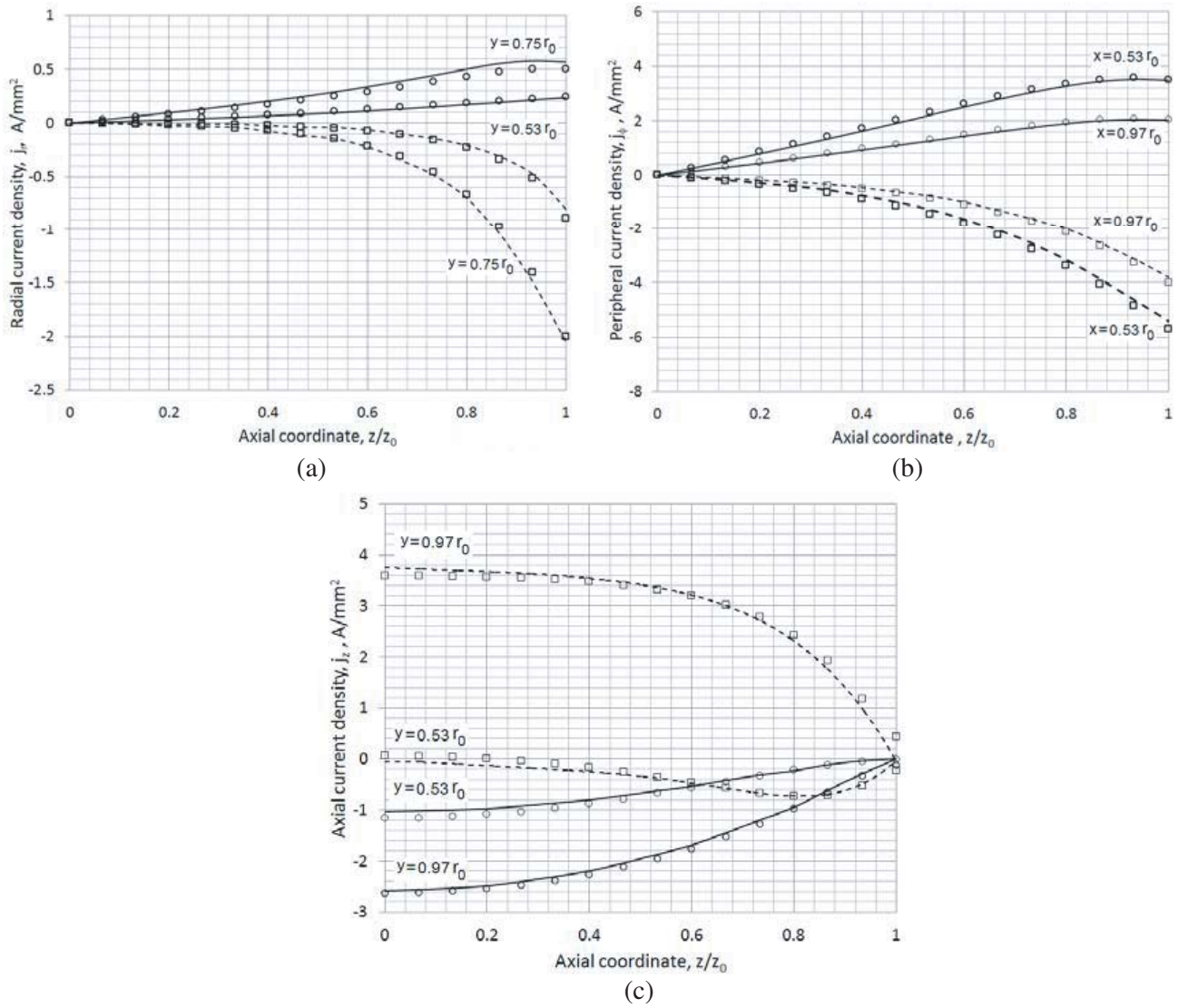

Figure 9. (a) Radial component of current density in YZ-plane, (b) peripheral component of current density in XZ-plane and (c) axial component of current density in YZ-plane across a hollow cylinder of $r_0 = 1\,\text{cm}$, $r_i = 0.5\,\text{cm}$, $z_0 = 1$ at $f = 300\,\text{Hz}$, $B_0 = 10\,\text{mT}$: solid line = realj_z, analytics, dash line = imaginaryj_z, analytics; $\circ$ = realj_z, FEA, $\square$ = imaginaryj_z, FEA.

frequencies are low, the field on the axis is in a good agreement with the accurate approximation of the shell by five layers ($N = 6$). When the frequency increases, the matrix condition number becomes too large, and the approximation in Eq. (85) at $N = 1$ starts to give us an inaccurate field on the axis. It should be noted that the calculation of q_k in (85) using a straight expression (41) gives a more accurate result since in the case of just one layer the derivative dA_r/dr in the expression for $div\vec{A}$ is hard to determine accurately.

The alternative solution for the thin shell can be derived using a concept of stream function [2] and a scalar magnetic potential [19–20]. The magnetic field is split into the applied field, $\vec{H}_0$, and the field from the eddy currents, $\vec{H}_e$, where the normal component of x-oriented field on the shell surface is $H_{0r} = H_0 \cos\phi$. Outside the cylindrical shell we can use the scalar magnetic potential U to calculate the field from the eddy currents $\vec{H}_e = -\nabla U$. The magnetic scalar potential satisfies the Laplace equation everywhere but the shell. The whole space along the radial coordinate is divided by the shell into two

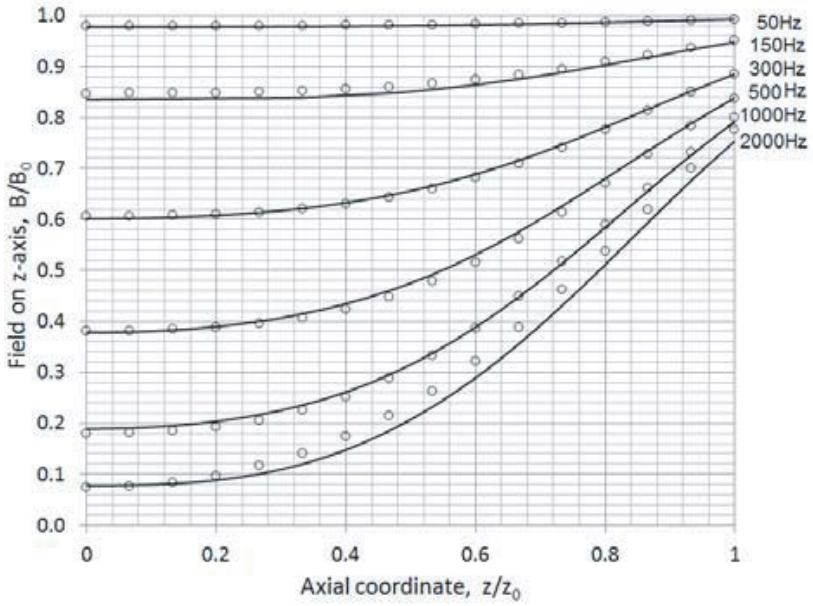

Figure 10. Field on axis of the hollow cylinder of $r_0 = 1\,\text{cm}$, $r_i = 0.5\,\text{cm}$, $z_0 = 1\,\text{cm}$ at different frequencies: solid line = analytics, $\circ$ = FEA.

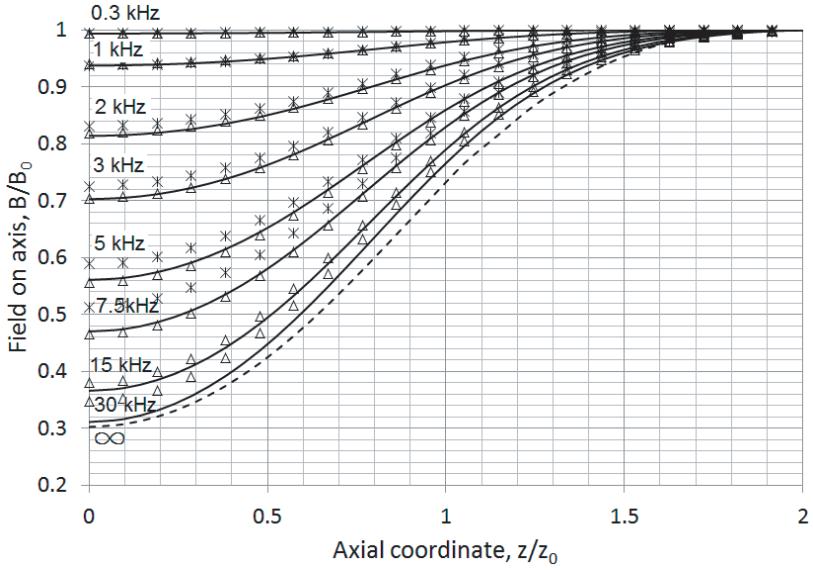

Figure 11. Field on axis of the cylindrical shell of $r_0 = 1\,\text{cm}$, $d_r = 0.35\,\text{mm}$, $z_0 = 1\,\text{cm}$ at different frequencies: solid line = 5 steps in radial grid, $* = V_k$ calculated per (85), Δ = scalar magnetic potential method per (99), dash line = superconducting shell.

regions: $r > r_0$ (marked by upper index +) and $r < r_0$ (marked by upper index −). The scalar potential inside (−) and outside (+) the shell can be written in terms of Bessel functions as

$$\begin{aligned} U^- &= \cos\phi \sum_{m=1}^{M} C_m^- I_1(\lambda_m r) \cos\lambda_m z, \\ U^+ &= \cos\phi \sum_{m=1}^{M} C_m^+ K_1(\lambda_m r) \cos\lambda_m z \end{aligned}, \tag{86}$$

where C_m^- and C_m^+ are the constants. Because the normal component of the field is continuous everywhere including the shell surface the constants in Eq. (86) are related as:

$$C_m^- I_1'(\lambda_m r_0) = C_m^+ K_1'(\lambda_m r_0). \tag{87}$$

The field tangential component has a jump by the amount of surface current density $\vec{j}_s = h_r \vec{j}$ when crossing the shell thickness from the inside to the outside

$$\vec{j}_s\Big|_{\substack{r=r_0 \\ 0\le z\le z_0}} = \vec{n} \times \left(\vec{H}_e^+ - \vec{H}_e^-\right). \tag{88}$$

The scalar magnetic potential also has a jump [16] on the shell surface $u = U^+ - U^-$. After expressing the field through the scalar magnetic potential in Eq. (88), one can write

$$\vec{j}_s\Big|_{\substack{r=r_0 \\ 0\le z\le z_0}} = \vec{n} \times (\nabla_s u), \tag{89}$$

where index s means that the nabla operator ∇_s works on the surface, and $\vec{n}$ is the unit vector normal to the surface.

In terms of components (89) can be rewritten as

$$j_{s\phi} = \frac{\partial u}{\partial z}, \quad j_{sz} = -\frac{1}{r_0}\frac{\partial u}{\partial \phi}. \tag{90}$$

In accordance with [2] the stream function $\Psi(\phi, z)$ relates to the current density as

$$\vec{j}_s = h_r \sigma \nabla_s \times \Psi \vec{n}, \tag{91}$$

or in terms of components

$$j_{s\phi} = h_r \sigma \frac{\partial \Psi}{\partial z}, \quad j_{sz} = -h_r \sigma \frac{1}{r_0}\frac{\partial \Psi}{\partial \phi}. \tag{92}$$

The stream function satisfies the equation

$$\frac{1}{r_0^2}\frac{\partial^2 \Psi}{\partial \phi^2} + \frac{\partial^2 \Psi}{\partial z^2} = i\omega\mu_0 H_r, \tag{93}$$

where H_r is the radial, i.e., component of the field normal to the cylindrical surface. Comparing Eq. (90) with Eq. (92), we can conclude that the potential jump u satisfies the equation similar to Eq. (93), namely

$$\frac{1}{r_0^2}\frac{\partial^2 u}{\partial \phi^2} + \frac{\partial^2 u}{\partial z^2} = i\omega\mu_0\sigma h_r H_r. \tag{94}$$

The potential jump u exists only at $r = r_0$ and $0 \le z \le z_0$, and it can be presented in the form of series

$$u = \cos\phi \sum_{m=1}^{M} u_m \cos \eta_m z. \tag{95}$$

After substitution Eq. (95) in Eq. (94) and integrating over $[0, z_0]$, the coefficients u_m are determined as follows:

$$u_m = -\frac{i\omega\mu_0\sigma h_r}{\left(\eta_m^2 + 1/r_0^2\right)}\frac{z_{\text{inf}}}{z_0}\left[d_{0m} + \sum_l \lambda_l b_{lm} C_l^- I_1(\lambda_l r_0)\right]. \tag{96}$$

The second equation for the coefficients C_m^- and u_m can be determined from the potential junction at $r = r_0$

$$U^- = \begin{array}{ll} U^+ - u & 0 \le z \le z_0 \\ U^+, & z_0 \le z \le z_{\text{inf}} \end{array}. \tag{97}$$

After integrating Eq. (97) over $[0, z_0]$ and substituting C_m^+ from Eq. (87), we obtain

$$C_m^- = \left[I_1(\lambda_m r_0) - K_1(\lambda_m r_0)\frac{I_1'(\lambda_m r_0)}{K_1'(\lambda_m r_0)}\right]^{-1} \sum_l b_{ml} u_l. \tag{98}$$

Equations (96) and (98) form the system of linear equations for the coefficients C_m^- and u_m that can be solved directly. However, Eqs. (96) and (98) can be solved by iterations with some under relaxation factor. We assume $C_m^- = 0$ for the first iteration, find u_m from Eq. (96) and update C_m^- using Eq. (98) with under relaxation. We iterate Eqs. (96) and (98) until the convergence tolerance is achieved. The iterative method implements the perturbation of the normal field H_r by the induced field starting with H_0 as a first approximation for the field on the shell surface. The iterative algorithm gives a more steady solution at high frequencies when the matrix of system in Eqs. (96) and (98) becomes ill defined.

The magnetic field on z-axis is calculated as

$$B_x\,|_{x;y=0} = -B_0 - \frac{1}{2}\sum_m \lambda_m C_m^- \cos(\lambda_m z). \tag{99}$$

The thin sheet approximation using the scalar potential works well even at high frequencies (Fig. 11). The discrepancy from the accurate solution ($N = 6$) increases at frequencies above 15 kHz when the shielding capacity of the shell is close to saturation. The solution in Eqs. (96) and (98) becomes unresponsive to the frequency because of difficulties in the accurate estimation of the normal component of the resultant field H_r on the shell surface (right part of Eq. (94)).

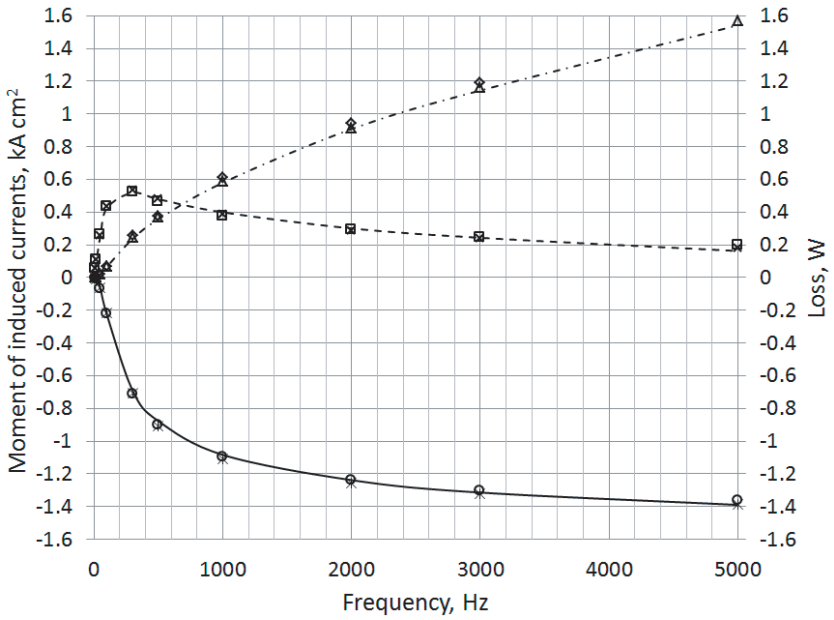

Figure 12. Moment of induced current and power loss in the solid cylinder of $r_0 = 1$ cm, $z_0 = 1$ cm at $B_0 = 10$ mT of transverse field: solid line = real$M$, analytics, dash line = imaginary$M$, analytics; $\circ$ = real$M$, FEA, $\square$ = imaginary$M$, FEA; $\times$ = real$M$, FDM, $*$ = imaginary$M$, FDM dash-dot line = power loss, analytics; Δ = power loss, FEA; $\Diamond$ = power loss, FDM.

4.4. Magnetic Moment and Power Loss

The magnetic moment M_x of currents induced in the cylinder is

$$M_x = 8\int_0^{\pi/2}\int_{r_i}^{r_0}\int_0^{z_0} (j_z r\sin\phi + j_y z)(rd\phi)drdz. \tag{100}$$

After substituting series (25)–(27) and integrating one can find

$$M_x = 2\pi\sum_{m=1}^{M}(-1)^{(m+1)}\left[\frac{1}{\eta_m}\sum_{n=1}^{N} j_{zm}(r_n)r_n^2 w_n h_{rn} + \frac{1}{\eta_m^2}\sum_{n=1}^{N}\left(j_{rm}(r_n) + j_{\phi m}(r_n)\right) r_n w_n h_{rn}\right]. \tag{101}$$

The power loss in the cylinder is

$$P = \frac{1}{2\sigma}\int_0^{2\pi}\int_{r_i}^{r_0}\int_0^{z_0}\left(j_r j_r^* + j_\phi j_\phi^* + j_z j_z^*\right) r dz dr$$
$$= \frac{\pi z_0}{2\sigma}\sum_{n=1}^{N}\sum_{m=1}^{M}\sum_{l=1}^{M}\left[c_{ml}^{-}\left(j_{rm}j_{rl}^* + j_{\phi m}j_{\phi l}^*\right) + c_{ml}^{+}j_{zm}j_{zl}^*\right] w_n r_n \Delta_{rn}. \quad (102)$$

where

$$c_{ml}^{\pm} = \frac{1}{z_0}\left(\frac{\sin(\eta_m - \eta_l)z_0}{\eta_m - \eta_l} \pm \frac{\sin(\eta_m + \eta_l)z_0}{\eta_m + \eta_l}\right).$$

The results of calculation of power loss and magnetic moment of the copper solid cylinder using Eqs. (101)–(102) in test models agree well with the data from FEA and FDM (Fig. 12).

5. CONCLUSION

The analytical solutions for the eddy current problem in the conductive solid and hollow cylinders in cases of axial and transverse fields have been derived. The separation of three components has been achieved in the equation for vector potential in cylindrical coordinates. The magnetic field outside the cylinder or inside the bore is expressed in terms of Bessel functions. Formulas have been verified by the comparison of the calculation results in test models with the FDM method and modern FEA codes. Formulas for the power loss and magnetic moment of currents induced in the cylinder have been also found. These have been validated over a wide range of frequencies within the limits of quasistatic approximation.

REFERENCES

1. Lameraner, J. and M. Štafl, *Eddy Currents*, Iliffe Books London, Ltd., 1966.
2. Knoepfel, H. E., *Magnetic Fields*, John Wiley & Sons, Inc, New York-Toronto, 2000.
3. Batygin, V. V. and I. N. Toptygin, *Problems in Electrodynamics*, problems 368 and 371, Academic, London, U.K., 1976.
4. Grimberg, R, E. Radu, O. Mihalache, and A. Savin, "Calculation of the induced electromagnetic field created by an arbitrary current distribution located outside a conductive cylinder," *J. Phys. D: Appl. Phys.*, Vol. 30, 2285–2291, 1997.
5. Brandt, E. H., "Superconductor disks and cylinders in an axial magnetic field. I. Flux penetration and magnetization curves," *Phys. Rev. B*, Vol. 58, No. 10, 6506–6522, 1998.
6. Lopez, H. S., M. Poole, and S. Crozier, "Eddy current simulation in thick cylinders of finite length induced by coils of arbitrary geometry," *Journal of Magnetic Resonance*, Vol. 207, 251–261, 2010.
7. Bowler, J. R. and T. P. Theodoulidis, "Eddy currents induced in a conducting rod of finite length by a coaxial encircling coil," *J. Phys. D: Appl. Phys.*, Vol. 38, 2861–2868, 2005.
8. Perry, M. and T. Jones, "Eddy current induction in a solid conducting cylinder with a transverse magnetic field," *IEEE Trans. on Magn.*, Vol. 14, No. 4, 227–231, 1978.
9. Fawzi, T. H., K. F. Ali, and P. E. Burke, "Eddy current losses in finite length conducting cylinders," *IEEE Trans. on Magn.*, Vol. 19, No. 5, 2216–2218, 1983.
10. Morisue, T. and M. Fukumi, "3-D eddy current calculation using the magnetic vector potential," *IEEE Trans. on Magn.*, Vol. 24, No. 1, 106–109, 1988.
11. Huang, Q. S., L. Krahenbuhl, and A. Nicolas, "Numerical calculation of steady-state skin effect problems in axisymmetry," *IEEE Trans. on Magn.*, Vol. 24, No. 1, 201–204, 1988.
12. Turner, L. R., et al., "Results from the FELIX experiments on electromagnetic effects of hollow cylinders," *IEEE Trans. on Magn.*, Vol. 21, No. 6, 2324–2328, 1985.

13. *International Electromagnetic Workshops: Test Problems*, Apr. 1986, available online: https://www.osti.gov/scitech/servlets/purl/7179128.
14. Grinberg, G. A., *The Selected Problems of Mathematical Theory of Electric and Magnetic Phenomena*, Acad. Sci. USSR, Moscow-Leningrad, Russia, 1948.
15. *Opera 2D, User Guide and Opera 3D, User Guide*, Cobham Technical Services, Vector Fields Software, Kidlington, UK, Mar. 2016.
16. Tamm, I. E., *Fundamentals of the Theory of Electricity*, MIR Publishers, Moscow, 1979.
17. Samarskiy, A. A., *Theory of Finite Difference Schemes*, Nauka, Moscow, 1977.
18. Zhilichev, Y., "Superconducting cylinder of finite length in transverse magnetic field," *Latvian Journal of Physics and Technical Sciences*, No. 5, 14–21, 2001.
19. Ancelle, B., A. Nicolas, and J. C. Sabonnadiere, "A boundary integral equation method for high frequency eddy currents," *IEEE Trans. on Magn.*, Vol. 17, No. 6, 2568–2570, 1981.
20. Poltz, J. and K. Romanowski, "Solution of quasi-stationary fields problems by means of magnetic scalar potential," *IEEE Trans. on Magn.*, Vol. 19, No. 6, 2425–2428, 1983.